Alexander-Brett and Fremont

http://www.jem.org/cgi/content/full/jem.20071677/DC1

SUPPLEMENTAL MATERIALS AND METHODS

DNA constructs, protein expression, and purification. Biotin-tagged hCCL2 (M64I) and hCXCL10 for cell staining were cloned into a customized pET28 vector, which was engineered to include a thrombin cleavage site, a BirA recognition sequence, and a 6-His tag at the C terminus with the sequence GSLVPRGSLNDIFEAQKIEWHERLEHHHHHH. After expression at 37°C in BL21-Codon plus (RIL) *E. coli* (Stratagene), inclusion bodies were harvested, washed as previously described (1), and dissolved in 6 M guanidine. The proteins were renatured by 10-fold dilution into 100 mM Tris (pH 8.5), 5 mM EDTA, 10mM PMSF, and 1 mM of oxidized and 10 mM of reduced glutathione, with stirring overnight at 4°C. The refolding reactions were exchanged into 20 mM Hepes (pH 7.5) before ion exchange on SP sepharose using a 0–1-M NaCl gradient in the same buffer. Human CCL2 used in SPR analysis was released from the tag by thrombin cleavage and purified by Ni-NTA to remove the cleaved tag (QIAGEN). The resulting protein was homogeneous by electrospray mass spectrometry, yielding a molecular mass of 8,619 D corresponding to the sequence $G^{1}QPD\ldots TPK^{70}$. Human CXCL10 and biotinylated heparin (mean molecular mass ~15 kD) used in SPR experiments were purchased from Invitrogen and EMD, respectively.

x-ray crystallography. Crystals of the M3–CCL2 and M3–XCL1 complexes were formed by hanging drop vapor diffusion using 1 μl of protein (at 15 mg/ml) and 1 μl of precipitant that consisted of 12% PEG-4000, 100 mM sodium acetate (pH 4.1), 200 mM $MgCl_2$ (M3–CCL2) and 10% PEG-8000, and 100 mM Tris (pH 6.1; M3–XCL1). For data collection, crystals were cryopreserved in precipitant solution containing 20% ethylene glycol and flash cooled at 100 degrees Kelvin.

SPR experiments. All experiments were conducted at 25°C under conditions of 20 mM Hepes (pH 7.4), 150 mM NaCl, and 0.005% Triton X-100, unless otherwise indicated. For M3–chemokine interaction analysis, M3 variants were immobilized on a CM5 sensor chip in 10 mM sodium acetate (pH 4.1) using standard amine coupling. A control cell was treated in the same manner using coupling buffer alone. Identical results were obtained using other immobilization methods, such as neutravidin capture of N-terminal biotinylated M3 protein.

Sensorgrams for M3–chemokine binding were influenced by mass-transport effects at low salt (≤500 mM) and were completely dominated by transport at 150 mM NaCl, as indicated by a linear rather than exponential association phase and an artificially extended dissociation phase. Mass transport effects indicate that the SPR signal is not simply explained by the chemical reaction at the surface but is also a function of the transport rate (k_t) for analyte delivery. Transport-limited SPR data have been successfully analyzed using two-compartment models that account for transport, which has extended the upper range of on rates that may be obtained by this method (2, 3).

M3–XCL1 binding kinetics were measured as a function of NaCl to analyze the salt dependence of this interaction and were run in standard Hepes running buffer with NaCl from 200 mM to 1.5 M. M3 was immobilized to levels of 300, 400, and 570 RU. 2–100 nM XCL1 was injected over the flow cells at 80 μl/min, and the surface was regenerated with 500 mM $CaCl_2$. Data were analyzed in BIAevaluation software (version 3.1; Biacore), using a 1:1 interaction model for 0.6–1.5 M NaCl and using a two-compartment 1:1 mass transport model for 0.2–0.5 M NaCl with a fixed $k_t = 1.75 \times 10^8\ s^{-1}$. The kinetic constants k_a^{app} and k_d^{app} were determined from the fit to the sensorgrams, and the K_D was independently determined from the ratio $K_D = k_d^{app}/k_a^{app}$ and by a nonlinear fit to the R_{eq} values ($K_{D(eq)}$), as appropriate. Experiments were repeated in triplicate, and constants were averaged for all three immobilization levels.

Salt-dependent binding experiments were also repeated in a separate experiment for a series of three ionic strengths using either NaCl or $MgCl_2$ to test whether the affinity varied for different salts. Data analysis was conducted as described, and $K_{D(eq)}$ was reported under both conditions for comparison.

To measure binding constants for $M3^{BBXB}$ at 150 mM NaCl, the mutant was immobilized to a level of 800 RU, and 20–600 nM XCL1 was injected over the chip at 40 μl/min. Kinetic and equilibrium constants were obtained using a 1:1 interaction model, and a relatively small (twofold) difference between equilibrium and kinetic-derived values supports the use of this model. However, a deviation between these values might be explained by more complex binding kinetics or inhomogeneous coupling to the chip. To measure wild-type M3–XCL1 affinity at 150 mM NaCl by competition, 20 nM XCL1 was preequilibrated with 0–60 nM M3 and injected in the same manner.

To measure chemokine binding to heparin and M3 competition, heparin sensor chips were prepared by neutravidin capture of biotinylated heparin. Neutravidin (Thermo Fisher Scientific) was coupled to a CM5 chip in 10 mM sodium citrate (pH 4.5) using standard amine chemistry. 15-kD heparin-biotin was injected at 5 mg/ml in Hepes running buffer with 300 mM NaCl and bound to a level of ~150–300 RU. A flow cell coupled with neutravidin alone was used as a control. Chemokines were injected over the heparin chip at 20 μl/min (CCL2) and 80 μl/min (XCL1 and CXCL10) to measure heparin binding, and the surface was regenerated using 1 M NaCl. The R_{eq} values (end of the association phase) were analyzed to determine K_D for each chemokine. For CCL2 and CXCL10, a 1:1 interaction model was used to fit the data, but for XCL1, marked positive coopera-

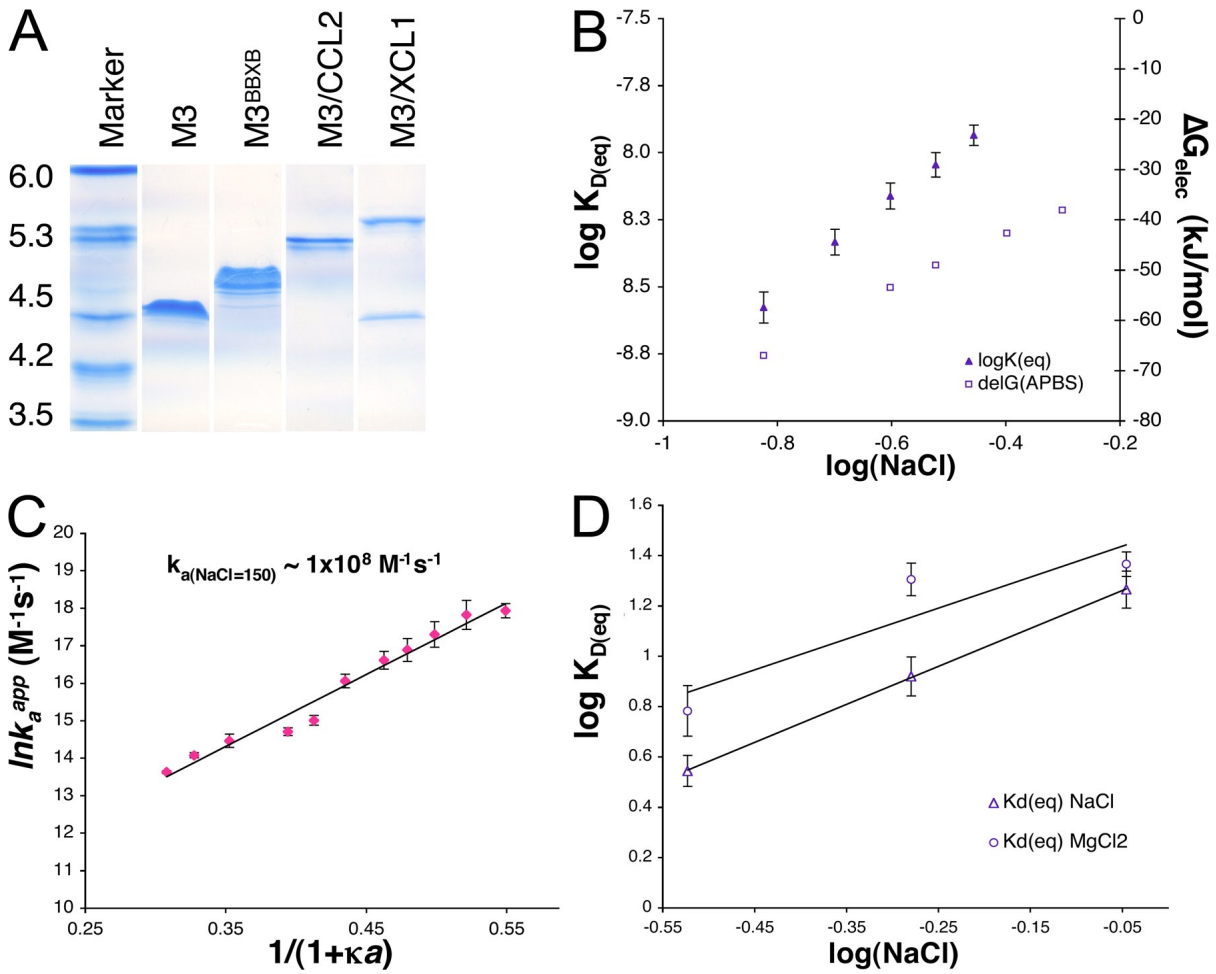

Figure S1. Electrostatic analysis of M3–XCL1 interactions. (A) Isoelectric focusing gel for M3, $M3^{BBXB}$, M3–monocyte chemoattractant protein 1 (1:1) and M3–XCL1 (1:1). pI standards are left of the marker lane. (B) Plot of M3–XCL1 log($K_{D(eq)}$) and the calculated electrostatic interaction energy from APBS (ΔG_{elec}) as a function of log NaCl. (C) Plot of M3–XCL1 $ln(k_a)$ versus 1/1 + κa and linear fit to the database on Debye-Huckel analysis; the extrapolated value for k_a^{app} at 150 mM NaCl is listed on the plot. (D) Salt dependence of M3–XCL1 $K_{D(eq)}$ as a function of ionic strength for NaCl versus $MgCl_2$. Error bars represent the mean ± SEM.

tivity was apparent; therefore, a cooperative oligomerization model previously described for RANTES binding to heparin (4) was used to estimate the K_D. M3 competition assays were performed as follows. 2.3 μM CCL2, 84 nM hCXCL10, and 120 nM XCL1 were preequilibrated with M3 over a range of 0.2–3 μM, 5–125 nM, and 0–220 nM, respectively. Each were injected over the heparin chip in the same manner as for chemokine alone.

Electrostatic calculations. The program APBS was used to calculate potential maps and electrostatic interaction energies (ΔG_{elec}) (5). PQR and APBS input files were generated using PDB2PQR (agave.wustl.edu) with PARSE partial charges. The linear Poisson-Boltzmann equation was solved for the M3–XCL1 complex and individual components at several ionic strengths using the automated multigrid method (solvent dielectric = 80, protein dielectric = 12, temperature = 298 degrees Kelvin). The solvent radius was set to 0 (van der Waals surface) for the molecular surface calculation. The electrostatic interaction energy (ΔG_{elec}) was calculated by subtracting the calculated PB energies of the individual components from the complex (Fig. S1 and Table S1).

Experimental determination of isoelectric points. For determination of experimental isoelectric points, samples containing 1 mg/ml M3, $M3^{BBXB}$, and M3 were premixed at a 1:1 molar ratio with chemokines. The complexes were then run on a Novex isoelectric focusing gel (pH 3–10), according to standard protocol (Invitrogen), and visualized using Coomassie blue staining (Fig. S1). The chemokines XCL1 and CCL2 were also analyzed but were found to completely run off the gel (caused by pI > 9.5; not depicted).

Electrostatic analysis of kinetics. Several protein–protein and protein–nucleic acid interactions exhibit salt-dependent kinetics, which have previously been analyzed according to the Debye-Huckel theory (6, 7), as well as theories based on specific protein–ion binding (8). Both of these approaches were considered during analysis of the salt dependence of M3–XCL1 binding kinetics.

The kinetic data were modeled using the Debye-Huckel theory similar to a previous study (7). This method assumes that a trend in k_a with increasing NaCl is purely an ionic strength effect in which bulk ions in solution shield electrostatic interactions between proteins, and does not account for specific protein–ion interactions.

For the Debye-Huckel electrostatic analysis, $ln(k_a)$ is plotted versus $1/1 + \kappa a$ (where κ^2 ($Å^{-2}$) is 0.108 times the ionic strength (M) at 298 K [9], using $a = 5.6$ Å as the minimal distance of approach [6]), and fit according to the following equation (7):

$$\ln k_a = \ln k_a^0 + \left(\frac{-\Delta G_{elec}}{RT}\right)\left(\frac{e^{-\kappa(r-a)}}{1+\kappa a}\right)$$

Table S1. Analysis of ionic strength effects on M3–XCL1 binding

I[a]	ΔG_{elec} APBS (kJ/mol)	$K_{D(eq)}$ NaCl (nM)	$K_{D(eq)}$ $MgCl_2$ (nM)
0	−355		
0.15	−67		
0.25	−53.5		
0.3	−49	3.5 (±0.8)	6 (±0.9)
0.4	−42.7		
0.5	−38.1		
0.53		9 (±1)	20 (±4)
0.6			
0.9		18 (±2)	23 (±4)

[a]Results of the following equation

$$I = \frac{1}{2}\Sigma m_i z_i^2,$$

where m is ion concentration in moles per liter and z is the valence.

The k_a is a function of the basal on rate $k^0{}_a$ in the absence of electrostatic enhancement and the electrostatic interaction energy (ΔG_{elec}), which decreases with increasing ionic strength according to $e^{-\kappa(r-a)}/(1+\kappa a)$, where r is set equal to a, as described previously (7). A plot of $ln(k_a)$ versus $1/1 + \kappa a$ was approximately linear over the entire range of salt concentration studied (Fig. S1). Therefore, a linear fit to this plot was extrapolated to yield an estimate for the M3–XCL1 k_a^{app} at 150 mM NaCl of $\sim 10^8$ $M^{-1}s^{-1}$.

The Debye-Huckel analysis described was conducted to estimate the M3–XCL1 association rate at salt concentrations that could not be obtained experimentally. However, a trend in on rate as a function of salt may also reflect competing processes such as specific ion binding to either protein (8). To test whether specific protein–ion binding may contribute to the on rate trend observed, measurements were conducted under the same ionic strength using either NaCl or $MgCl_2$. The results show small differences in affinity (less than twofold) for the two salts at each concentration tested, indicating that some degree of specific protein–ion binding may occur in this system (Fig. S1 and Table S1). This result suggests that the trend in M3–XCL1 on rate may not be fully described by the shielding of electrostatic interactions from bulk ions in solution but may involve a more complex process in which bound ions are released from the protein surfaces upon M3–XCL1 binding. In either case, the results of these analyses clearly demonstrate the importance of electrostatics in the enhancement of M3–XCL1 interactions.

SPR competition assay. Equations used to analyze competition titrations were derived as follows (Eqs. 1–6), assuming a 1:1 interaction for both the receptor on the chip and the solution competitor (A = total analyte, M = receptor on chip, M*=competitor in solution), and affinities for the chip-bound receptor and the solution-phase competitor denoted as K_M and K_{M*}, respectively:

$$M^*A \xleftarrow{K_{M^*}} M^* + A + M \xleftarrow{K_M} MA$$

The expression for analyte binding to the chip-bound receptor and the solution competitor are 1:1 Langmuir binding models (10):

$$\frac{R}{R_{\max}} \propto \frac{MA}{M_{tot}} = \frac{K_M A_{free}}{1 + K_M A_{free}} \quad (1)$$

$$\frac{M^*A}{M^*_{tot}} = \frac{K_{M^*} A_{free}}{1 + K_{M^*} A_{free}} \quad (2)$$

Total analyte is the sum of free, receptor-bound and competitor-bound analyte:

$$A_{tot} = A_{free} + M^*A + MA \quad (3)$$

Assuming that analyte is in large excess over the receptor on the chip, A_{tot} simplifies to:

$$A_{tot} = A_{free} + M^*A \text{ (in the absence of } M^*,\ A_{tot} = A_{free}) \quad (4)$$

Substituting Eq. 2 into Eq. 4 yields Eq. 5, which can be solved for free analyte to obtain an expression that describes free analyte concentration as a function of solution competitor:

$$A_{tot} = A_{free} + \left(\frac{K_{M^*} A_{free}}{1 + K_{M^*} A_{free}}\right) M^*_{tot} \quad (5)$$

$$A_{free} = -\frac{1}{2K_{M^*}}\left(\left(-A_{tot}K_{M^*} + M^*_{tot}K_{M^*} + 1\right) - \sqrt{\left(\left(A_{tot}K_{M^*} - M^*_{tot}K_{M^*} - 1\right)^2 + 4A_{tot}K_{M^*}\right)}\right) \quad (6)$$

Competition titration curves were fit to Eqs. 1 and 6 using the program Scientist to yield the dissociation constant ($K_I = 1/K_{M^*}$) for M3 binding to chemokines in competition with the chip-bound receptor.

REFERENCES

1. Frayser, M., A.K. Sato, L. Xu, and L.J. Stern. 1999. Empty and peptide-loaded class II major histocompatibility complex proteins produced by expression in *Escherichia coli* and folding in vitro. *Protein Expr. Purif.* 15:105–114.
2. Myszka, D.G., X. He, M. Dembo, T.A. Morton, and B. Goldstein. 1998. Extending the range of rate constants available from BIACORE: interpreting mass transport-influenced binding data. *Biophys. J.* 75:583–594.
3. Schuck, P., and A.P. Minton. 1996. Analysis of mass transport-limited binding kinetics in evanescent wave biosensors. *Anal. Biochem.* 240:262–272.
4. Vives, R.R., R. Sadir, A. Imberty, A. Rencurosi, and H. Lortat-Jacob. 2002. A kinetics and modeling study of RANTES(9-68) binding to heparin reveals a mechanism of cooperative oligomerization. *Biochemistry.* 41:14779–14789.
5. Baker, N.A., D. Sept, S. Joseph, M.J. Holst, and J.A. McCammon. 2001. Electrostatics of nanosystems: application to microtubules and the ribosome. *Proc. Natl. Acad. Sci. USA.* 98:10037–10041.
6. Schreiber, G., and A.R. Fersht. 1996. Rapid, electrostatically assisted association of proteins. *Nat. Struct. Biol.* 3:427–431.
7. Selzer, T., and G. Schreiber. 1999. Predicting the rate enhancement of protein complex formation from the electrostatic energy of interaction. *J. Mol. Biol.* 287:409–419.
8. Lohman, T.M. 1986. Kinetics of protein-nucleic acid interactions: use of salt effects to probe mechanisms of interaction. *CRC Crit. Rev. Biochem.* 19:191–245.
9. Debye, P., and E. Hückel. 1923. Zur Theorie der Elektrolyte. *Physiol. Zeitschr.* 24:185–206.
10. Schuck, P. 1997. Use of surface plasmon resonance to probe the equilibrium and dynamic aspects of interactions between biological macromolecules. *Annu. Rev. Biophys. Biomol. Struct.* 26:541–566.